Classification
Physics Abstracts
61.16D — 61.70 — 74.70V

High resolution electron microscopy study of the high T_c superconductor $Tl_{0.5}Pb_{0.5}Sr_4Cu_2CO_3O_7$

Maryvonne Hervieu, Claude Michel, Marielle Huvé, Christine Martin, Antoine Maignan and Bernard Raveau

Laboratoire CRISMAT-ISMRA, Université de Caen, Bd. du Maréchal Juin, 14050 Caen Cedex, France

(Received 28 December 1992, accepted 3 March 1993)

Abstract. — The structure and the microstructure of the new high T_c superconductor $Tl_{0.5}Pb_{0.5}Sr_4Cu_2CO_3O_7$ have been studied by high resolution electron microscopy. The experimental images fit well with the calculated ones based on a structure built up from the intergrowth of a 1201-type slice $[Tl_{0.5}Pb_{0.5}Sr_2CuCO_5]_\infty^{1201}$ with a $[Sr_2CuCO_3O_2]_\infty$ unit. The comparison of the calculated and experimental images with those of a 1223 structure, which exhibits similar cell parameters to those of $Tl_{0.5}Pb_{0.5}Sr_4Cu_2CO_3O_7$, shows that the oxycarbonate exhibits a characteristic contrast for some focus values which allows to differentiate the two structures. The investigation of numerous crystals attests of the high regularity of the stacking of the layers along **c**. One single type of defect was observed which suggests the possible existence of a new member $[Tl_{0.5}Pb_{0.5}Sr_2CuO_5]\,[Sr_2CuCO_3O_2]_2$.

1. Introduction.

The possibility to introduce CO_3 groups in the perovskite structure [1] is at the origin of the synthesis of new superconductors built up from perovskite layers, deficient or not, connected through rows of carbonate groups. This is the case of the 66 K-superconductor $(Y_{1-x}Ca_x)_{0.95}Sr_{2.05}Cu_{2.4}CO_3O_y$ [2] and of the 40 K-superconductor $(Ba_{1-x}Sr_x)_2Cu_{1+y}O_{2+y+z}(CO_3)_{1-y}$ [3] which belong to the structural series $(Y, Ca)_n(Ba, Sr)_{2n}Cu_{3n-1}CO_3O_{7n-3}$ [4-6] and $A_{2n}Cu_{2n-1}CO_3O_{5n-3}$ [7-8] respectively. The recent discovery of the 70 K-superconductor $Tl_{0.5}Pb_{0.5}Sr_4Cu_2CO_3O_7$ [9] is of interest since it is the oxycarbonate with the highest T_c and the highest Meissner volume fraction (70%) synthesized up to now. The preliminary structural study of this phase has shown that it is derived from the thallium cuprates previously studied for their superconducting properties, so that it belongs to a new series with the generic formula $(Tl, Pb)_nSr_{4n}Cu_{3n-1}CO_3O_{10n-3}$. Thus, the knowledge of this phase is of capital importance for the generation and the optimization of the other members of the series. We report here on the HREM study of this new oxycarbonate.

2. Experimental.

The samples were prepared as previously mentioned [9] from a mixture of oxides and carbonate, according to the nominal composition $Tl_{0.5}Pb_{0.5}Sr_4Cu_2CO_3O_7$, pressed in the form of bars. The

bars were sealed in evacuated ampoula, introduced in a furnace at 900°C, heated for 6 hours and quenched down to room temperature.

The E.D. study was performed with JEOL 120 CX and 200 CX E.M. fitted with a side entry goniometer (±60°) and high resolution electron microscopy with a TOPCON 002 B electron microscope operating at 200 kV; the lens aberration constant is 0.4 mm. The samples were prepared by a smooth crushing of the oxycarbonate in n butanol, deposited on a holey carbon film supported by an aluminium grid. The theoretical images were calculated using E.M.S. program [10]. The EDX analysis was performed with KEVEX analysers mounted on both JEM 200 CX and TOPCON electron microscopes.

3. Structure recall.

A first model of the oxycarbonate was proposed from HREM images and XRD calculations [9]. In spite of the low scattering factors of oxygen and carbon atoms which hinter accurate positional parameters to be determined, the following description can be proposed for the average structure. It is built up from the intergrowth of double rock salt layers $[(Tl_{0.5}Pb_{0.5}O)\,(SrO)]_\infty$ with single $[SrCuO_3]_\infty$ perovskite layers, linked through single carbonate layers as shown in figure 1. The stacking of the layers along **c** involves the following sequence of the cations: [-($Tl_{0.5}Pb_{0.5}$)-Sr-Cu-Sr-C-Sr-Cu-Sr-]. This structure can be described also, in a simple way, as an intergrowth of 1201-type slices, $[Tl_{0.5}Pb_{0.5}Sr_2CuO_5]_\infty$, with $[Sr_2CuO_2CO_3]_\infty$ units.

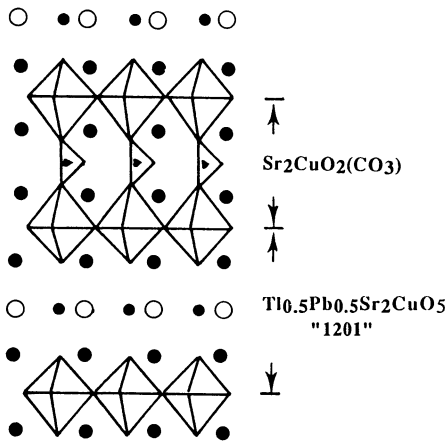

Fig. 1. — [Idealized drawing of the structure of $Tl_{0.5}Pb_{0.5}Sr_4Cu_2CO_3O_7$.]

4. Results.

The E.D. investigation attests of the homogeneity of the sample. The reconstruction of the reciprocal space evidences a tetragonal cell with $a \sim a_p \sim 3.80$ Å and $c \sim 16.5$ Å, without systematic absence of reflection. The [001] and [100] E.D. patterns are given in figure 2. The examination

of numerous crystals shows that neither extra reflections nor diffuse streaks appear in the E.D. patterns.

The overall images confirm the highly regular stacking of the layers along **c**. Such an image which is typical of most of the crystals is shown in figure 3a. Clearly, one does not observe intergrowth defects or local disordering phenomena, which would break down the regularity.

The comparison of this image, enlarged in figure 3b, with the HREM image of the 1223 cuprate $Tl(Ba,Sr)_2Ca_2Cu_3O_{10}$ [11] (Fig. 3c) shows clear relationships between the two structures. One recognizes three rows of white spots characteristic of double rock salt layers $[(TlO)(SrO)]_\infty$ or $[(TlO)(Ba,SrO)_\infty]_\infty$ in both images. The three rows of grey spots corresponding to the triple copper layers in the 1223-structure (Fig. 3c) are replaced by only two rows of grey spots in $Tl_{0.5}Pb_{0.5}Sr_4Cu_2CO_3O_7$ (Fig. 3b), with a strong variation of the contrast at the level of the intermediate layer (curved arrow), suggesting that the copper atoms of the latter have been replaced by lighter atoms, i.e. carbon of CO_3 groups.

The EDX analysis was performed on several crystals, taking as references $Tl_{0.5}Pb_{0.5}Sr_2Ca_2Cu_3O_{11}$, Sr_2CuO_3, $Sr_4Tl_2O_7$ and $SrPbO_3$. This analysis leads to the cationic composition "$Tl_{0.5}Pb_{0.5}Sr_4Cu_2$" which is in agreement with the nominal composition and shows the copper deficiency with respect to the "1223" compound ($Tl_{0.5}Pb_{0.5}Sr_2Ca_2Cu_3$).

Theoritical images were calculated on the basis of the positional parameters refined from XRD data (Tab. I). The through focus series calculated for a crystal thickness of 31 Å is shown in figure 4. An image where the dark spots are correlated to the position of the cations, close to the Scherzer value, is shown in figure 5; the nature of the different layers is indicated on the right part of the image. It appears, in agreement with the calculated image, that the Scherzer value does not provide the most meaningful image for evidence the carbonate layers. In fact, the images recorded for −20 nm, −50 nm and −85 nm focus values appear as the most characteristic of the oxycarbonate structure; they are shown in figures 6a to c respectively, and compared with the calculated ones. For $\Delta f \sim -50$ nm (Fig. 6b) the cations appear as white dots; the rows of brightest dots correspond to $[Pb_{0.5}Tl_{0.5}]_\infty$ layers, whereas the darkest rows correspond to $[CO]_\infty$ layers (Fig. 6b). For the two other Δf values, the triple rows of intense white spots can be correlated with light electronic density zones; they correspond to triple layers of oxygen atoms, belonging to the triple layers, $[(SrO)(CO)(SrO)]_\infty$. Such triple layers form the rows of CO_3 groups so that they can be formulated $[Sr_2CO_3]_\infty$.

This structure can be described as derived from an hypothetical structure $Tl_{0.5}Pb_{0.5}Sr_4Cu_3CO_{10}$ (Fig. 7a) closely related to that of the 1223. The latter would be built up from two octahedral copper layers linked through $[CuO_2]_\infty$ rows of square planar groups. In order to check that the observed contrast does not correspond to this hypothetical structure, images were calculated for this model. The positions used for such calculations are deduced from the ideal interatomic distances using the structural results previously obtained for the 1223-cuprates [11-13]. The calculated images are shown is figure 7b; small variations in the cations positions were tested without any significant change of the contrast. These calculated images, especially for $\Delta f \sim -20$ nm, −50 and −85 nm values, show that a significant difference of contrast results from the substitution of the copper polyhedra by carbonate groups. The hypothesis of the formation of a "1223" cuprate can thus be discarded, in agreement with the EDX analyses.

This shows that the triple layers $[Sr_2CO_3]_\infty$, characteristic of the oxycarbonates, can be easily imaged by HREM. Thus the comparison between the observed and calculated images attests of the validity of the structural model proposed for $Tl_{0.5}Pb_{0.5}Sr_4Cu_2CO_3O_7$ (Fig. 1).

Although the layer stacking can be, as previously mentioned, considered as highly regular, some rare stacking defects are observed. Two examples are shown in figures 8 and 9. In these images, the rows of brighest dots are correlated to the presence of the oxygen atoms of the CO_3 groups, i.e. correspond to the triple layers $[Sr_2CO_3]_\infty$. In the largest part of these crys-

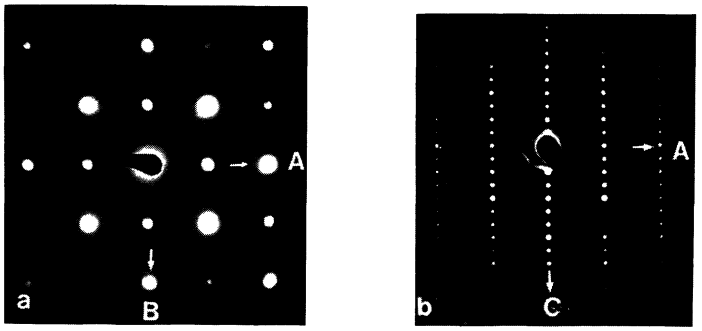

Fig. 2. — [a) [001] and b) [010] electron diffraction patterns.]

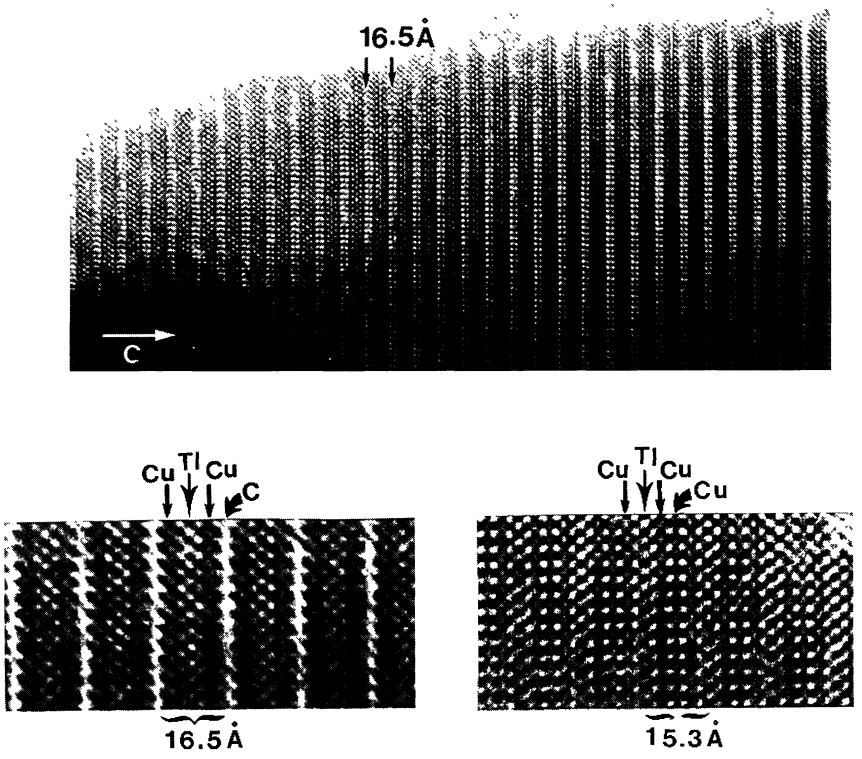

Fig. 3. — [a) [010] overall image of the $Tl_{0.5}Pb_{0.5}Sr_4Cu_2CO_3O_7$ phase showing the high regularity of the layer stacking along c. b) [010] enlarged image: the $[CO]_\infty$ layers (curved arrow) appears as a row of intense bright dots. c) comparison with a [010] enlarged experimental image of a 1223 phase for the same focus value. The $[CuO_2]_\infty$ layers appear as row of gret dots (curved arrow).]

Table I. — *Refined parameters obtained for* $Tl_{0.5}Pb_{0.5}Sr_4(CO_3)Cu_2O_7$. *Calculations were carried out in the space group P4/mmm.* $a = b = 3.8244$ [1] Å, $c = 16.516$[1]Å.

	Site	x/a	y/b	z/c
Tl/Pb	4l[(a)]	0.083(2)	0	0
Sr_1	2h	1/2	1/2	0.1596(2)
Sr_2	2h	1/2	1/2	0.3725(2)
Cu	2g	0	0	0.2654(3)
C	1b	0	0	1/2
O(1)	4n[(a)]	0.670(10)	1/2	0
O(2)	2g	0	0	0.121(1)
O(3)	8s[(a)]	0.162(7)	0	0.414(2)
O(4)	4n[(a)]	0.316(12)	0	1/2
O(5)	4i	1/2	0	0.277(1)

[(a)] occupancy factor $\tau = 0.25$.

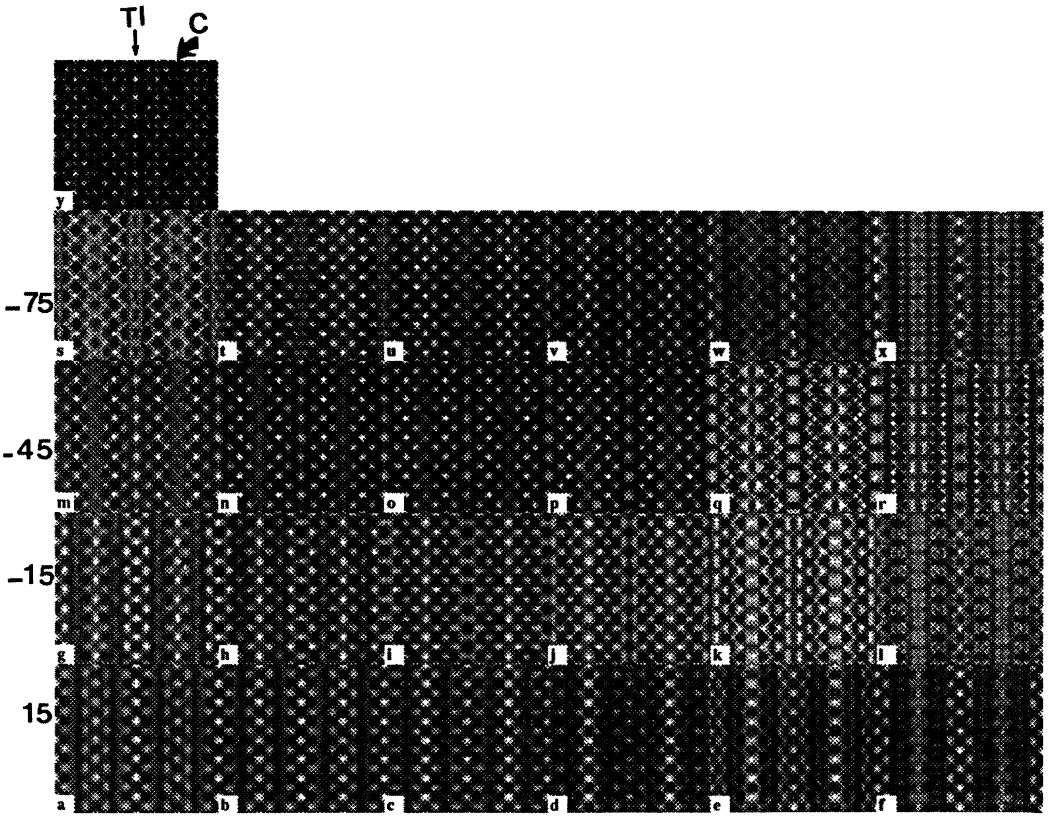

Fig. 4. — [$Tl_{0.5}Pb_{0.5}Sr_4Cu_2CO_3O_7$: [010] calculated through focus series. Calculation parameters are: high voltage $V = 200$ kV, spherical aberration $Cs = 0.4$ mm, half-angle convergence $\alpha = 0.8$ mrad, spread of focus $s = 12$ nm, crystal thickness $T = 3.1$ nm. Focus varies from a) + 15 to x) − 100 nm (by 5 nm step); y) projected potential.]

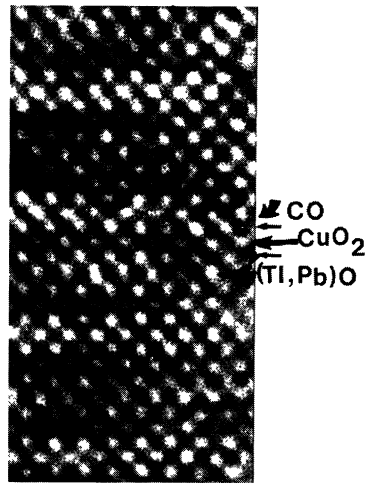

Fig. 5. — [Enlarged [010] experimental image where the dark spots are correlated to the cations positions. The (Tl, Pb)O is indicated by a black triangle, [SrO] by small arrows, $[CuO_2]_\infty$ by large black arrow and [CO] layer by curved arrow.]

tals these brighest rows are regularly spaced of 16.5 Å, corresponding to the stacking sequence "$Sr_2CO_3CuO_2-Tl_{0.5}Pb_{0.5}Sr_2CuO_5$" which consists of a regular intergrowth of one single (Sr_2CO_3 CuO_2)-type slice with one single 1201-type layer. In some parts of the crystals additional rows of bright dots are observed, leading either to isolated defects (Fig. 8 see arrows) or pair of defects (Fig. 9a see arrows), which are characterized by a much shorter distance of two successive rows bright dots of 7.5 Å. The enlarged image at the level of these defects (Fig. 9b) suggests that it is built up from the stacking of the different layers according to the following sequence:

$$\text{"SrO} - \text{CuO}_2-\text{SrO} - \text{CO} - \text{SrO} - \text{CuO}_2-\text{SrO} - \text{CO} - \text{SrO} - \text{CuO}_2-\text{SrO"}$$

instead of "SrO – CuO_2–SrO – CO – SrO – CuO_2–SrO" in the regular sequence of the oxycarbonate $Tl_{0.5}Pb_{0.5}Sr_4Cu_2CO_3O_7$. In order to check this structural hypothesis, we have calculated the theoritical images corresponding to such a sequence. The calculations were made on the basis of positional parameters deduced from those of $Tl_{0.5}Pb_{0.5}Sr_4Cu_2CO_3O_7$ (9), keeping on the Sr – O, Cu – O and C – O interatomic distances for the additional $Sr_2CuO_2CO_3$ slices. The calculated image for $\Delta f \sim -15$ nm, where the thallium positions appear as black dots (thin arrow) and the carbon positions as weak grey dots surrounded by four bright dots, is superposed to the experimental image in figure 9b. The comparison between the two images allows to confirm the proposed structural model.

This means that an additional layer with the composition and structure of $Sr_2CuO_2CO_3$ has been introduced into the matrix. This suggests the possible existence of a new member $Tl_{0.5}Pb_{0.5}Sr_2CuO_5$ $(Sr_2CuO_2CO_3)_2$, whose structure (Fig. 10) corresponds to the intergrowth of single 1201 layers with double $Sr_2CuO_2CO_3$-type layers. Such an oxycarbonate represents the member $n = 1$ $m = 2$ of the intergrowth with generic formula $[ASr_2CuO_5]_n^{1201}$ $[Sr_2CO_3CuO_2]_m$ (A = Tl, Pb). The parameter of the tetragonal cell of the different members of this intergrowth series can easily be calculated from those of the parent structures: $a = b \sim a_p \sim 3.8$ Å $c \approx (n.c_{1201} = m \times 7.5)$ Å i.e. $c \approx (9 \times n + 7.5 \times m)$Å.

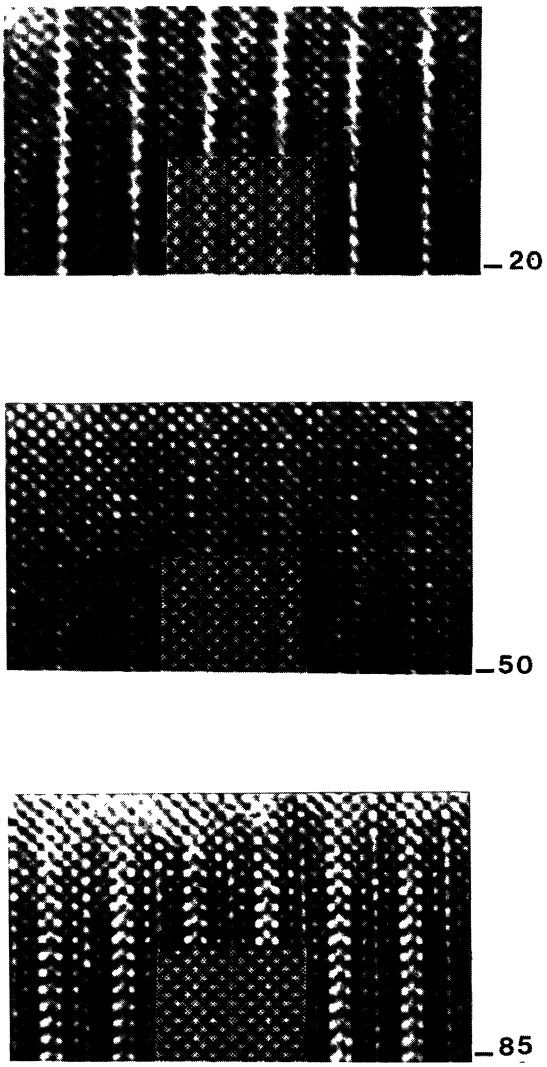

Fig. 6. — [Comparison between experimental and calculated images for Δf = a) −20 nm, b) −50 nm and c) −85 nm for the $Tl_{0.5}Pb_{0.5}Sr_4Cu_2CO_3O_7$ phase.]

5. Concluding remarks.

The HREM study of the oxycarbonate $Tl_{0.5}Pb_{0.5}Sr_4Cu_2CO_3O_7$ shows that, despite the short heating time and the quenching process, the complex stacking of the different layers along the **c** axis is ensured in a regular manner. The rare intergrowth defects which have been observed are of a single type. They can be described as the "$n = 1$, $m = 2$" members of the family $[Tl_{0.5}Pb_{0.5}Sr_2CuO_5]_{\infty}^{1201}\,[Sr_2CuCO_3O_2]_m$.

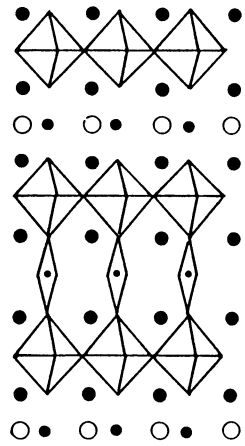

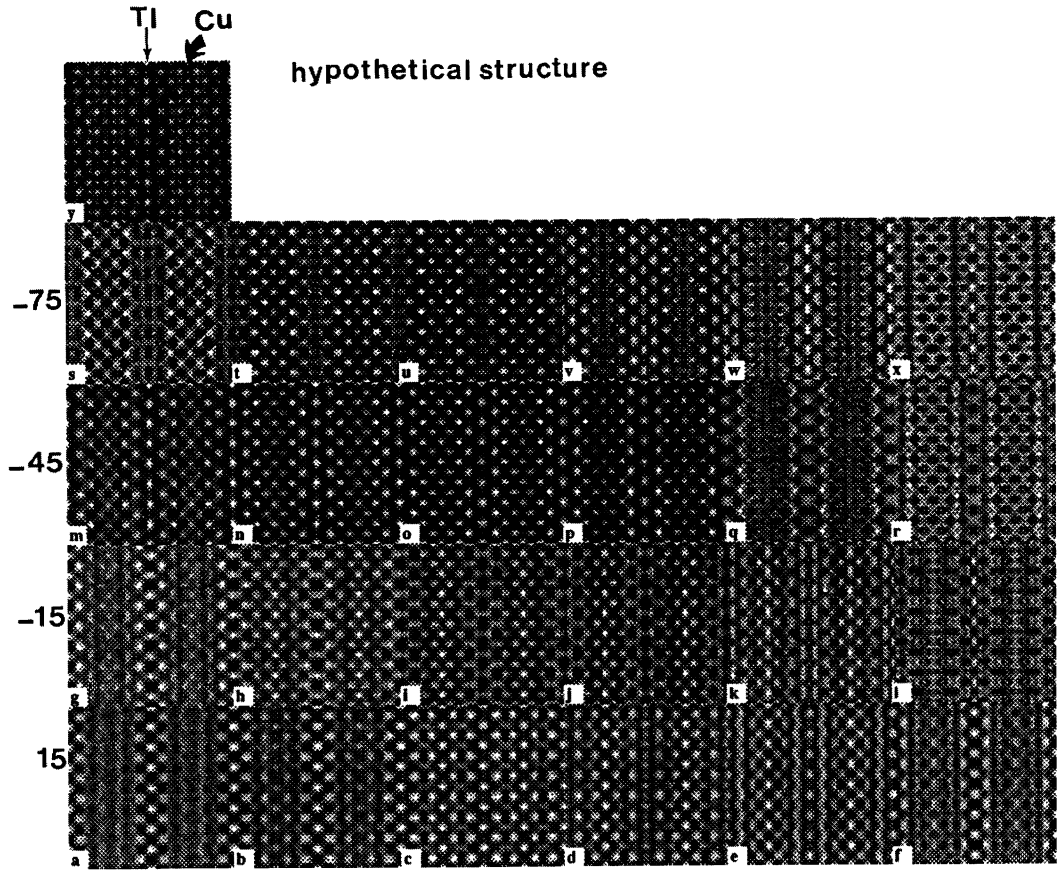

Fig. 7. — [a) idealized drawing of the hypothetical $Tl_{0.5}Pb_{0.5}Sr_4Cu_3O_{10}$ b) example of calculated images for a 1223-type structure. The calculation parameters are those of figure 7. On the projected potential (y), Cu intermediate layer is curved arrowed.]

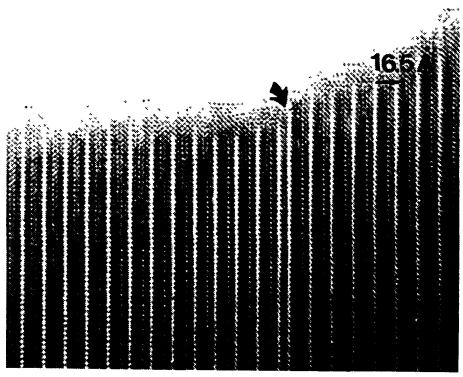

Fig. 8. — [Example of a single defect in a [010] image (curved arrow).]

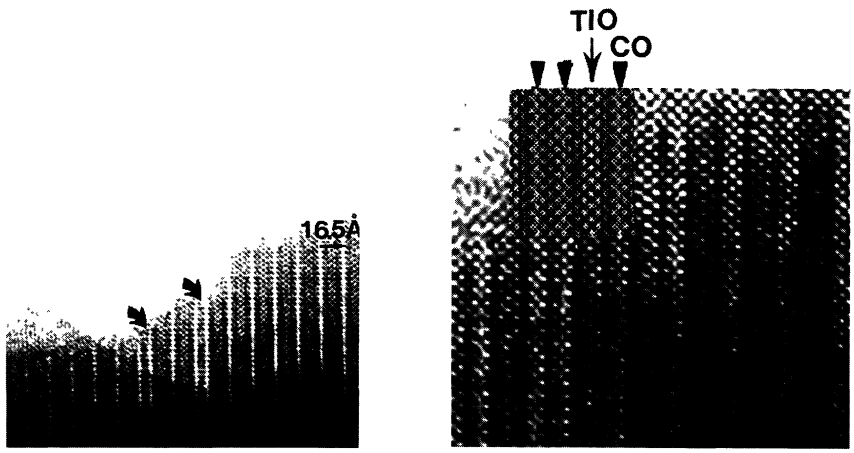

Fig. 9. — [a) example of a double defect. b) enlargement of the image (recorded for a focus value of −15 nm) showing the layer stacking at the level of the defect. The calculated image, based on the model proposed in figure 10, is superposed on the top of the micrograph.]

References

[1] GREAVES C. and SLATER P.R, *Physica C* **175** (1991) 172.
[2] ADIMITSU J., VEHARA M., OGAWA M., NAKATA H., TOMINOTO K., MIYAZAKI Y., YAMANE H., HIRAI T., KINOSHITA K. and MATSUI Y., *Physica C* **201** (1992) 320.
[3] KINOSHITA K. and YAMADA Y., *Nature* **357** (1992) 312.
[4] MIYAZAKI Y., YAMANE H., OHNISHI N., KAJITANI T., HIRAGA K., MORII Y., FUNAHASHI S.and HIRAI T., *Physica C* **198** (1992) 7.
[5] HERVIEU M., BOULLAY Ph., DOMENGÈS B., MAIGNAN A. and RAVEAU B., submitted to J. Solid State Chem.
[6] DOMENGÈS B., HERVIEU M. and RAVEAU B., *Physica C* **207** (1993) 65.
[7] IZUMI F., KINOSHITA K., MATSUI Y., YAMADA K.T. and ASANO H., *Physica C* **196** (1992) 227.
[8] MIYAZAKI Y., YAMANE H., KAJITANI T., OKU T., HIRAGA K., MORII Y., FUCHISAKI K., FUNAHASHI S. and HIRAI T., *Physica C* **191** (1992) 434.

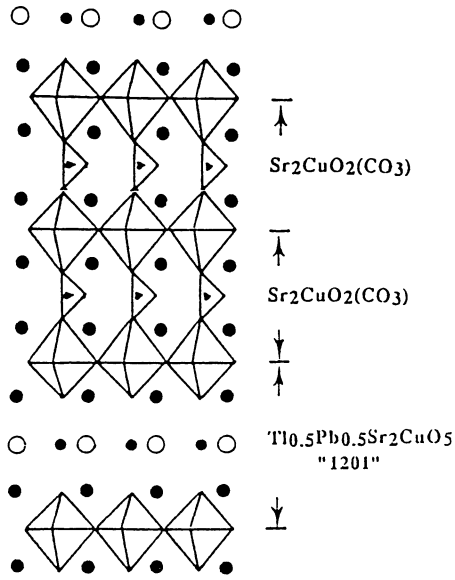

Fig. 10. — [Idealized model of the defect, corresponding to a $(Tl_{0.5}Pb_{0.5}Sr_2CuO_5)$ $(Sr_2CuO_2CO_3)_2$ member.]

[9] HUVÉ M, MICHEL C., MAIGNAN A., HERVIEU M., MARTIN C. and RAVEAU B., *Physica C* **205** (1993) 219.
[10] STADELMAN P., *Ultramicroscopy* **14** (1981) 149.
[11] MARTIN C., HUVÉ M., HERVIEU M., MAIGNAN A., MICHEL C. and RAVEAU B., *Physica C* **201** (1992) 362.
[12] TORARDI C.C., CALABRESE M.A., GOPALAKRISNAN J.C., Mc CARRON E.M., MORRISSEY K.J., ASKEW T.R., FLIPPEN R.B., CHAWDRY U., SLEIGHT A.W., *Science* **240** (1988) 631.
[13] PARISE J.B., GAI P.L., SUBRAMANIAN M.A., GOPALAKRISNAN J. and SLEIGHT A.W., *Physica C* **159** (1989) 245.